A triple-resonance Raman chip for simultaneous enhancement of Stokes and anti-Stokes lines utilizing both localized and non-localized plasmonic resonance



2015 J. Opt. 17 105001

(http://iopscience.iop.org/2040-8986/17/10/105001)

IOP Publishing Journal of Optics
J. Opt. 17 (2015) 105001 (7pp) doi:10.1088/2040-8978/17/10/105001

# A triple-resonance Raman chip for simultaneous enhancement of Stokes and anti-Stokes lines utilizing both localized and non-localized plasmonic resonance

**Jiao Lin[1], Yuan Zhang[2], El-Hang Lee[1] and Sailing He[1,2,3]**

[1] State Key Laboratory of Modern Optical Instrumentations, Centre for Optical and Electromagnetic Research, Zhejiang University, Hangzhou 310058, People's Republic of China
[2] ZJU-SCNU Joint Research Center of Photonics, Centre for Optical and Electromagnetic Research, South China Academy of Advanced Optoelectronics, South China Normal University (SCNU), 510006 Guangzhou, People's Republic of China
[3] Department of Electromagnetic Engineering, School of Electrical Engineering, Royal Institute of Technology (KTH), S-100 44 Stockholm, Sweden

E-mail: sailing@kth.se

Received 17 May 2015, revised 30 June 2015
Accepted for publication 8 July 2015
Published 21 August 2015

**Abstract**

In this paper we report a triple-resonance surface-enhanced Raman scattering (SERS) chip that is able to provide simultaneous field enhancement for both the Stokes and anti-Stokes lines. The structure consists of an array of periodic gold bowties placed on the surface of a uniform gold film. It can support two localized surface plasmonic resonances (LSPRs): an electric dipole binding resonance (EDBR) and a magnetic dipole resonance (MDR). A third field enhancement peak is obtained by utilizing the strong interaction between the non-localized surface plasmonic resonance (non-localized SPR) and the LSPR, which greatly raises the field enhancement for the non-localized SPR. In addition, a gold strip-line resonator is incorporated to further enhance the local field intensity. Consequently, the field enhancement of the three peaks are all increased. Compared with the same structure without strip, the periodic bowtie-strip compound structure on gold film can gain as much as ~22.8 times and ~3.6 times larger Raman intensity enhancement simultaneously for both the Stokes and anti-Stokes lines.

Keywords: triple-resonance, Raman enhancement, surface plasmonic resonance

## 1. Introduction

Raman scattering is the inelastic scattering process between a photon and a molecule, mediated by a fundamental vibrational or rotational mode of the latter [1, 2]. The scattered photon energy can both shift up (anti-Stokes) and down (Stokes) due to the energy exchange between the scattering partners. Raman scattering is extremely weak since only a small fraction of photons (approximately one in 10 million) are inelastically scattered. As a result, surface-enhanced Raman spectroscopy (SERS) is proposed to hugely increase the Raman scattering by exploiting the highly localized near field of the metallic nano-structures [3, 4]. Metallic nanostructures that support plasmonic resonances can concentrate light into a deep-subwavelength region and thus the local near field can be much larger than the incident field [5]. The enhancement factor in SERS is proportional to the product of the intensity enhancement at the excitation frequency and that at the scattering frequency [4]. It becomes a usual $E^4$ dependence on the EM field when the Raman excitation and scattering are very close to each other in spectrum [6].

Various types of metallic nano-structures are used as SERS substrates in the early stage, such as metallic electrodes with rough surfaces [7], metallic nano-particles in solutions [8], metal covered nanostructures [9] and so on. With the development of nanolithography methods, planar metallic

 

structures attract much more attention in SERS detection because of their high reproducibility compared to other SERS structures [10]. Among them, triangular-shaped nanoparticles in a tip-to-tip configuration, the so-called bowtie, demonstrate outstanding performance in SERS due to the gap mode and the lightning-rod effect [11, 12]. It has been demonstrated experimentally that high-quality bowtie structure (sharp tips, small gaps under 10 nm and high uniformity) can be precisely manufactured by the state-of-the-art electron beam lithography (EBL) technology on different substrates [12–15].

Most of these metallic nano-structures support one single resonance, which is enough for Raman enhancement when the Raman emission is near to the excitation in frequency. However, when the energy difference between the Raman emission and excitation is large, typical applications like SERS detection in long wave number (for example, C-H vibration, ~3000 $cm^{-1}$) or surface enhanced nonlinear Raman scattering, such as surface enhanced hyper Raman scattering (SEHRS) [16, 17], the performance of single-resonance plasmonic structures in these cases would be largely limited by the bandwidth. Besides, in some applications, the intensity ratio of anti-Stokes over Stokes signals are required to obtain information on laser heating effect [18], molecule vibrational pumping [19] and so on. To meet the large field enhancement requirements in these applications, a triple-resonance SERS chip is put forward to provide simultaneous field enhancement at the frequencies of the excitation, Stokes and anti-Stokes scattering. Such a triple-resonance SERS chip can also work in a dual-resonance condition with two major EM field enhancement peaks to provide enhancement to both the excitation and the Raman scattering.

As we know, there are two types of plasmonic resonances: the localized surface plasmonic resonance (LSPR) and the non-localized surface plasmonic resonance (non-localized SPR) [6]. Our triple-resonance SERS chip is achieved by utilizing both the LSPRs and the non-localized SPR, especially the strong interaction between them. We start with a periodic gold bowtie structure placed on a uniform gold film. It has been known that two LSPRs are supported in this structure, i.e. the electric dipole binding resonance (EDBR) and the magnetic dipole resonance (MDR) [14]. However, in our study, it has been found that, besides the two LSPRs, a non-localized SPR can also be excited on the corrugated surface of the periodic structures when the wave vector is matched. At the same time, by changing the period of the bowtie array, strong interaction can be induced between the LSPRs and the non-localized SPR when their resonant frequency gets near to each other [20–23]. By utilizing the strong interaction, three electric field enhancement peaks can be achieved and thus can be used to simultaneously enhance the Stokes and anti-Stokes lines.

Moreover, to further enhance the field intensity of the gold bowtie SERS chip, a gold strip-line resonator is integrated with the bowtie to couple more light into the 'hot spot' (the position with the highest field intensity). It has been found as a result that the field intensities of all the three plasmonic resonances can be simultaneously increased by the added gold strip-line. However, the degree of enhancement for each peak varies quite differently. For example, the enhancement effect of the gold strip-line on the EDBR is very minor compared to that on the MDR. This is because the MDR is a sub-radiant resonance and thus the strip-line can not only couple more incident light into the hot spot, but also can increase the excitation efficiency of the mode. More interestingly, the field intensity of the non-localized SPR can both be increased and decreased by the strip-line according to the width of the strip-line. By way of optimization of the width, it has been demonstrated that the bowtie-strip can provide Raman intensity enhancement simultaneously on both the Stokes and anti-Stokes lines at 1800 $cm^{-1}$, by as much as ~22.8 times and ~3.6 times larger than that provided by the same gold bowtie array without the strip-line. Meanwhile, when the gold bowtie-strip array grew on gold film structure works in dual-resonance condition, for example, to enhance Stokes signal at 3000 $cm^{-1}$, the Raman intensity enhancement of the new bowtie-strip array structure can achieve $10^8$, twice as large as the same structure without the gold strip, one order in magnitude larger than that of the single bowtie structure on gold film (also support two LSPR resonances) and two orders of magnitude larger than other single-resonance bowtie structures, including the free-standing bowtie array and the bowtie array/50 nm glass/gold film structures.

## 2. Results and discussion

We perform the finite-difference-time-domain (FDTD) simulations using a commercially available software package (Lumerical Solutions, Inc. [24]) to understand the optical properties of the non-localized SPR. The schematic of the structure is shown in figure 1(a) with magnified unit cell (enclosed in dashed box) shown in the inset. The bowtie structure has an arm length (L) of 0.12 $\mu$m, thickness (T) of 0.055 $\mu$m, apex angle ($\theta$) of 50°, and gap size (g) of 0.01 $\mu$m. The radii (r) of the curve at constituent triangle tips are set to be 0.015 $\mu$m. The grating constant is set to be 0.8 $\mu$m to let in the higher order non-localized SPR. Ther of the bowtie along the *x*-axis on the uniform gold surface. The field enhancement (normalized by the correspondie direction along the bowtie arm is set to be the *x*-axis, and the *y*-axis is chosen perpendicular to arm length in the bowtie plane. In the simulation, the plane wave is used as the excitation source incident from the top with electric field polarized along the *x*-axis. The boundary conditions in the *x*- and *y*-axes are set to be periodic and set to be perfect matched layers (PMLs) in the *z*-axis. The mesh size is 0.5 nm which is much smaller than the element sizes and the operating wavelength. The complex dielectric constant of gold is taken from the experimental data reported in [25]. The whole structure is placed in a vacuum environment. The tolerance of our structure is numerically investigated. It is found that the resonant frequencies and field enhancement of both LSPRs are largely influenced by the variation of the gap size and only the MDR is influenced by the thickness. Both LSPRs show little dependence on structure parameters including the round corner radii and the arm

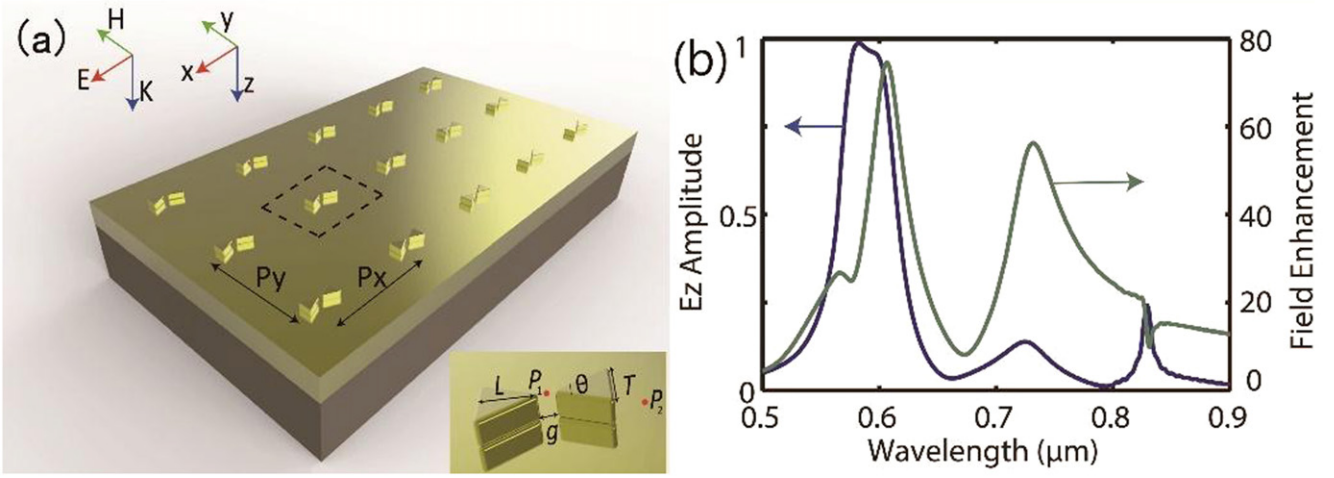


**Figure 1.** (a) A schematic diagram of the gold bowtie array structure on a uniform gold film is shown with structure parameters shown in the inset; L = 0.12 $\mu$m, T = 0.055 $\mu$m, $\theta = 50°$, g = 0.01 $\mu$m, r = 0.015 $\mu$m, $P_x = P_y = 0.8$ $\mu$m; (b) the green curve represents the field enhancement at point $P_1$ and the blue curve corresponds to the $E_z$ amplitude at point $P_2$.

length. Thus, in the experiment, the gap size and the thickness need to be precisely controlled [26, 27]. Two point monitors are placed to detect the electric field. One point monitor $P_1$ is placed on the top surface of the bowtie and in the middle of the gap. The other point monitor $P_2$ is placed a quarter period away from the centng electric field when the plane wave illuminates the same space without the whole structure) spectrum at $P_1$ is shown in figure 1(b) (the green curve) with two distinct peaks at 0.607 $\mu$m and 0.732 $\mu$m, which correspond to the EDBR and MDR, respectively. Besides the two LSPRs, the non-localized SPR can also be excited in the corrugated surface when the wave vector is matched. Assuming that the dispersion properties of the non-localized SPR are not disturbed by the corrugated surface, the resonant wavelength of the non-localized SPR on the smooth metal–air interface can be approximated by the following equation according to momentum conservation at normal incidence [28].

$$\lambda(\mathrm{m},\ \mathrm{n}) = \frac{1}{\sqrt{\left(\frac{m}{P_x}\right)^2 + \left(\frac{n}{P_y}\right)^2}} \sqrt{\frac{\varepsilon_m \varepsilon_{\mathrm{air}}}{\varepsilon_m + \varepsilon_{\mathrm{air}}}} \qquad (1)$$

where, $\varepsilon_m$ and $\varepsilon_{\mathrm{air}}$ are the permittivity of the metal and the air, respectively, and m and n are integers that represent the diffraction order along the x and y axes, respectively. According to equation (1), the resonant wavelengths of the non-localized SPR (1, 0) and (1, 1) are 0.817 $\mu$m and 0.578 $\mu$m, respectively. As a result, the two minor dips at 0.829 $\mu$m and 0.582 $\mu$m in the field enhancement spectrum just represent the (1, 0) and (1, 1) non-localized SPR. To confirm this, the $E_z$ field amplitude at $P_2$ (the field maximum position of the non-localized SPR) is shown (the blue curve) in figure 1(b). As expected, distinct peaks are observed at the two resonant frequencies corresponding to the two minor dips in the field enhancement spectrum. The dips in the field enhancement spectrum are an interaction result with the adjacent LSPRs, which will be extensively studied in the following part.

To extensively study the interaction between the LSPRs and the non-localized SPR, the spectra of the field enhancement at point $P_1$ is scanned with $P_x$ from 0.3 $\mu$m to 0.8 $\mu$m. In figure 2, two distinct field enhancement peaks can be observed when $P_x$ is small, which correspond to the EDBR at the shorter wavelength and the MDR at the longer wavelength. As $P_x$ increases, another field enhancement peak appears, for which its resonant frequency changes linearly with $P_x$. The third enhancement peak is contributed by the (1,0) order non-localized SPR. When $m = 1$, $n = 0$, and $\varepsilon_{\mathrm{air}} = 1$, we have:

$$\lambda(1,\ 0) = P_x \sqrt{\frac{\varepsilon_m}{\varepsilon_m + 1}} \qquad (2)$$

The dashed white lines in figure 2 are drawn according to equation (2). It can be seen that the theoretical results represented by the dashed white line actually indicate a reasonably good match to the numerically calculated resonant frequency of SPR in the linear region. However, when the resonant frequency of the non-localized SPR approaches that of the EDBR and the MDR, an obvious anti-crossing behavior of the resonance positions appear due to a strong interaction between the LSPRs and the non-localized SPR. By utilizing the strong interaction, three enhancement peaks can be achieved to simultaneously enhance the Stokes and anti-Stokes lines, and this effect will be further discussed later. In addition to an influence on the resonant frequency, the field enhancement is also affected by the strong mode interaction. Clearly, the maximum field enhancement appears when the non-localized SPR is under a strong interaction with the LSPRs. However, the large increase in the field enhancement of the non-localized SPR is accompanied by a decrease in the field enhancement of both the EDBR and the MDR, which indicates that the resonant energy is actually transferred from both the LSPRs to the non-localized SPR through the

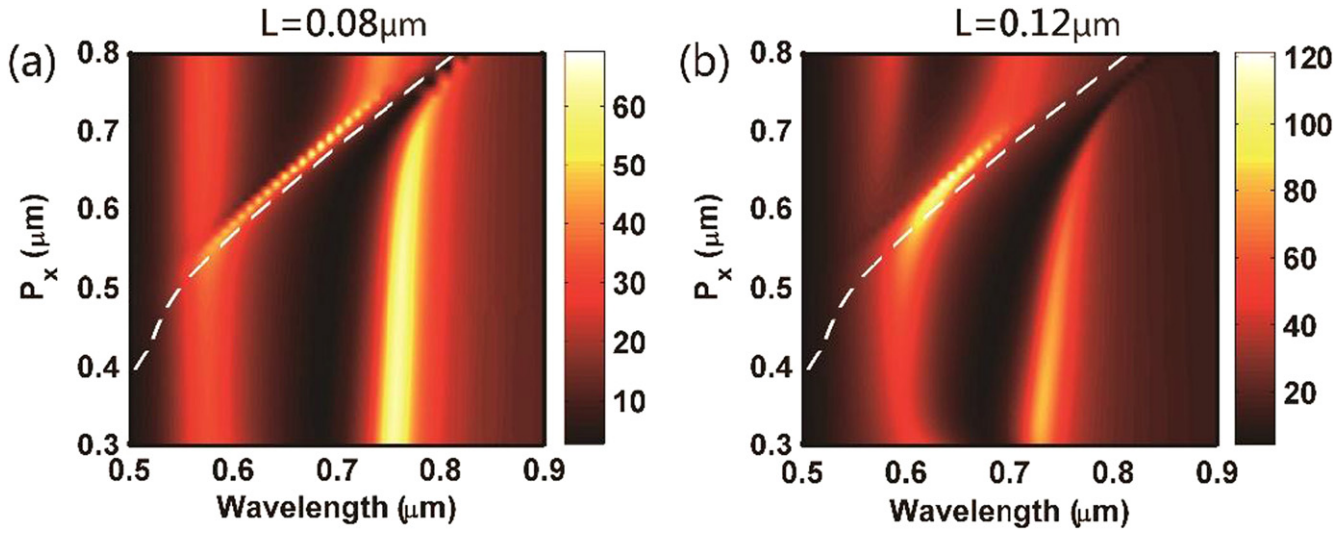


**Figure 2.** Two dimensional field enhancement spectra of the gold bowtie array structure with (a) L = 0.08 $\mu$m and (b) L = 0.12 $\mu$m. The schematic of the bowtie: T = 0.055 $\mu$m, $\theta$ = 50°, g = 0.01 $\mu$m, r = 0.015 $\mu$m, $P_y$ = 0.4 $\mu$m.

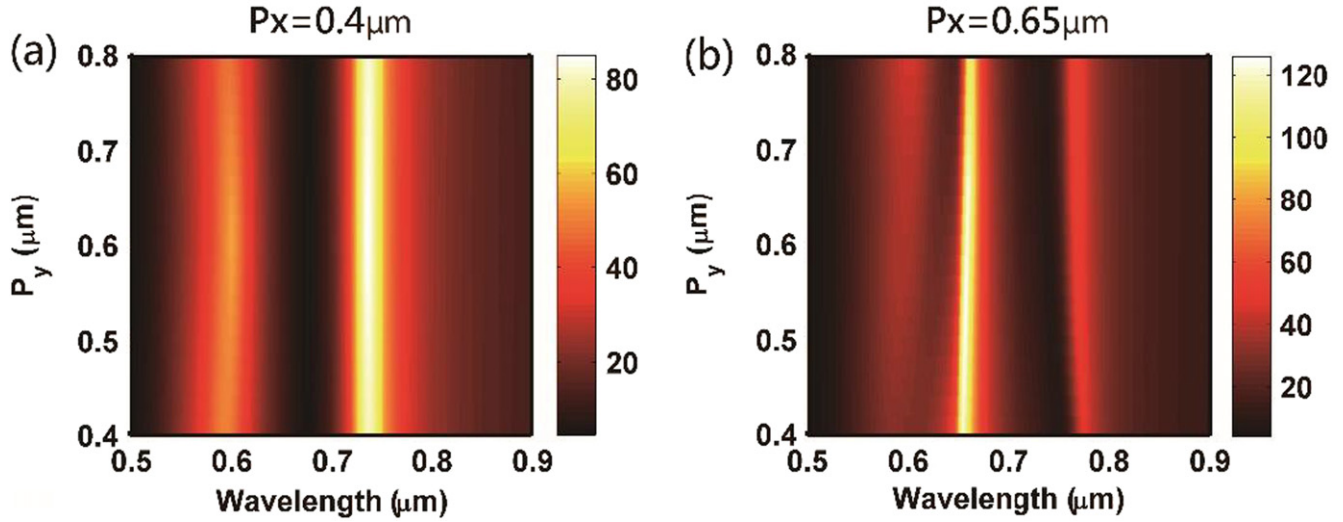


**Figure 3.** Two-dimensional field enhancement spectra of the gold bowtie array structure with (a) $P_x$ = 0.4 $\mu$m and (b) $P_x$ = 0.65 $\mu$m. The schematic of the bowtie: L = 0.12 $\mu$m, T = 0.055 $\mu$m, $\theta$ = 50°, g = 0.01 $\mu$m, r = 0.015 $\mu$m, $P_y$ = 0.4 $\mu$m.

interaction between them. In figure 2(b), when $P_x$ equals 0.3 $\mu$m, the resonant frequencies of the EDBR and the MDR red and blue shift, respectively, due to a formation of the binding and anti-binding mode with the neighboring bowtie [29]. This binding mode can further increase the field enhancement of the EDBR while the anti-binding mode decreases the field enhancement of the MDR.

In figure 3, the field enhancement spectra is studied in the same way as that in figure 2 with $P_y$ being scanned from 0.4 $\mu$m to 0.8 $\mu$m. In contrast, the resonant frequencies of both the LSPRs and (1,0) SPR are hardly shifted. In figure 3(a), it is seen that the field enhancements of both the EDBR and the MDR vary very little. However, in figure 3(b), three enhancement peaks are observed due to the strong mode interaction. Moreover, the field enhancement of the EDBR and the MDR increases while that of the non-localized SPR decreases. From the previous discussion, we have already known that the strong mode interaction would lead to the resonant energy transformation from the LSPRs to the non-localized SPR. Thus, it is believed that the interaction strength between the non-localized SPR and the LSPRs decreases with an increase in $P_y$.

In order to further increase the field intensity of the triple/dual-resonance plasmonic Raman chip, a gold strip-line resonance is integrated with the bowtie. The schematic of the bowtie-strip array/gold film structure is shown in figure 4(a). The direction of the gold strip is perpendicular to the long axis of the bowtie. A careful attention must be paid to distinguish between our gold bowtie-strip structure placed directly on gold film and the three layer structure having a dielectric spacer between the above antenna and the mirror ground [30, 31]. Despite the similarity in the structure, the resulting optical spectrum is quite different. With a dielectric spacer, only one LSPR can be excited. Dual-resonance can

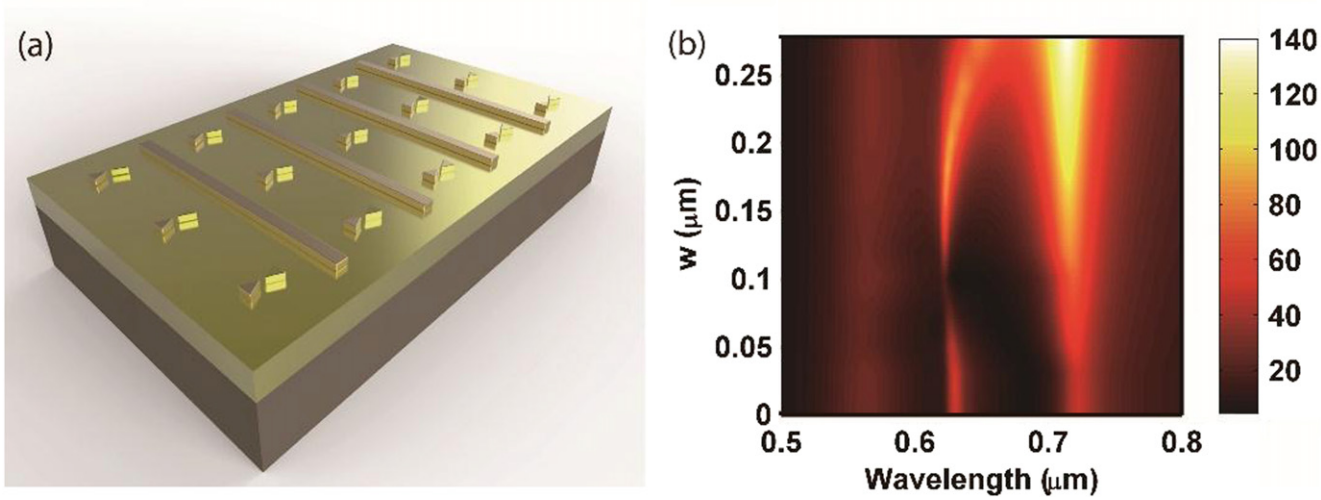


**Figure 4.** (a) The schematic of the gold bowtie-strip array on uniform gold film; (b) field enhancement spectra of the gold bowtie-strip array when the width of the strip-line increases; L = 0.08 $\mu$m, T = 0.048 $\mu$m, $\theta = 50°$, g = 0.01 $\mu$m, r = 0.015 $\mu$m, $P_x = 0.62$ $\mu$m, $P_y = 0.4$ $\mu$m.

only be achieved by strong interaction with the non-localized SPR supported in the ground mirror. The maximum number of the field enhancement peaks are two at most. However, by removing the dielectric spacer, two independently tunable LSPRs can be excited simultaneously and three enhancement peaks can be achieved in our chip. Moreover, the function of the strip-line is more complex here. In [28], a strip-line is mainly used to increase the radiation directivity as well as to couple more light into the hot spot. In our structure, however, besides the two functions, the strip-line can also be used to increase the excitation efficiency of the MDR. So the maximum intensity enhancement for one peak provided by the strip-line is ~6.8 times, which is much larger than that reported in [28].

In figure 4(b), the field enhancement spectra are shown for the case when the width of the strip-line is steadily increased. It shows that the field enhancement of the MDR increases quickly as the strip-line width increases wider and wider. The reason behind this effect is clear. When the width of the strip-line increases, the light coupling ability is also increased and thus more incident light can be coupled into the hot spot, thereby increasing the field enhancement. However, the increasing rate of the field enhancement of the EDBR is much slower compared to that of the MDR. This is because the MDR is a sub-radiant mode and thus the strip-line can not only couple more incident light into the hot spot but also can greatly increase the excitation efficiency of the mode by introducing more scattering. More interestingly, the field enhancement of the non-localized SPR varies with the width of the strip-line. The maximum and minimum peaks in the field enhancement is attributed to the constructive and destructive interference between the directly excited and the reflected non-localized SPR. Meanwhile, as can be seen, when the width is larger than 0.25 $\mu$m, the resonant frequency of the non-localized SPR shows a clear red-shift, leading to a relatively broad enhancement region.

From the previous discussion, it can be seen that the three field enhancement peaks can be achieved by a strong interaction between the non-localized SPR and the LSPRs. Thus, the resonant frequency of the three peaks can be carefully tuned to simultaneously enhance the excitation, Stokes and anti-Stokes lines. The EDBR and MDR provide the field enhancement to the anti-Stokes line and Stokes line, respectively. The non-localized SPR provides the field enhancement to the excitation wavelength. Here, the excitation wavelength is chosen to be at 0.633 $\mu$m. The Stokes and anti-Stokes lines are at 0.715 $\mu$m and 0.568 $\mu$m, respectively, corresponding to a wave number of about 1800 $cm^{-1}$. In figure 5(a), it is seen that both the bowtie array and bowtie-strip can be used to realize this function. However, the enhancement abilities are quite different. By integration with an optimized strip-line (red line), it is found that three enhancement peaks can all be increased. The total Raman intensity enhancement of the bowtie-strip array on the Stokes and anti-Stokes lines are ~22.8 and ~3.6 times larger than that on the gold bowtie array without the strip-line (both structures are on gold film).

In figure 5(b), the gold bowtie structure is designed to enhance the Stokes line at ~3000 $cm^{-1}$. It is seen that the bowtie-strip array grew on gold film (green curve) provides two distinct field enhancement peaks and the total Raman intensity enhancement can be over $10^8$ in the middle of the 10 nm gap. Compared to the same structure without the gold strip (cyan curve), the Raman enhancement factor is twice larger. Compared to the single bowtie on uniform gold film (black curve), which also support the two LSPRs, the total Raman enhancement factor is increased by one order in magnitude. The field enhancement spectra of other single-resonance structures, including the free standing bowtie array (blue curve) [14] and the bowtie array/50 nm glass/gold film (red curve) [30], are also shown for comparison. It can be calculated that the total Raman enhancement factor of both single-resonance bowtie structures is two orders in magnitude lower than that of the bowtie-strip array grew on uniform gold film.

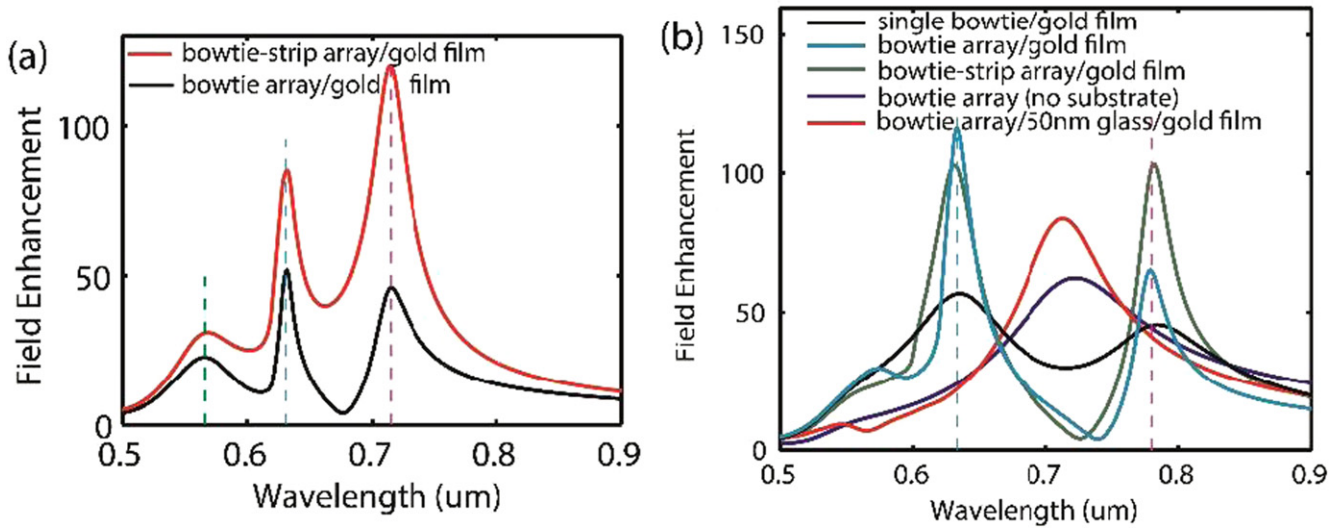


**Figure 5.** The field enhancement spectra of (a) triple-resonance: the black line represents the bowtie array/gold film and the red line represents the bowtie-strip array/gold film with w = 0.22 $\mu$m; other parameters are the same: $L = 0.08$ $\mu$m, $T = 0.048$ $\mu$m; $P_x = 0.62$ $\mu$m, $P_y = 0.4$ $\mu$m; dashed cyan, green and purple lines mark the position of the excitation, anti-Stokes and Stokes lines at ~1800 $cm^{-1}$; (b) dual/single-resonance: the field enhancement spectra of single bowtie/gold film with L = 0.16 $\mu$m, T = 0.062 $\mu$m (black); bowtie array/gold film with L = 0.12 $\mu$m, T = 0.058 $\mu$m, $P_x = 0.62$ $\mu$m (cyan); bowtie-strip array/gold film with L = 0.14 $\mu$m, $T = 0.06$ $\mu$m, $P_x = 0.6$ $\mu$m, strip width w = 0.1 $\mu$m, strip thickness $T_s = 0.06$ $\mu$m (green); bowtie array without substrate with L = 0.12 $\mu$m, T = 0.03 $\mu$m, $P_x = 0.4$ $\mu$m (blue); bowtie array/50 nm glass/gold film with $L = 0.08$ $\mu$m, T = 0.03 $\mu$m, $P_x = 0.4$ $\mu$m (red). The dashed blue and purple line represents the excitation wavelength at 0.633 $\mu$m and the Stokes line at 0.78 $\mu$m.; dashed cyan and purple lines mark the position of the excitation and Stokes lines at ~3000 $cm^{-1}$; all the other parameters are the same: $\theta = 50°$, g = 0.01 $\mu$m, $P_y = 0.4$ $\mu$m, r = 0.015 $\mu$m.

## 3. Conclusion

In conclusion, a triple-resonance plasmonic Raman chip is achieved for the first time using a gold bowtie array placed on a uniform gold film. The three enhancement peaks are provided collectively by the EDBR, the non-localized SPR and the MDR. It is to be noted that the field enhancement peak of the non-localized SPR can only be observed when it strongly interacted with the LSPR. A strong interaction occurs when the resonant frequency of the non-localized SPR approaches that of the LSPR, leading to a clear anti-crossing behavior. The resonant frequency of the non-localized SPR can be tuned by controlling the period of the gold bowtie structure. Moreover, a gold strip-line is additionally implemented to the gold bowtie structure in order to further increase the local near field. The gold strip can simultaneously increase the field enhancement of all the three modes by carefully choosing the width of the strip-line. It has been demonstrated that the new bowtie-strip structure proposed here can provide Raman intensity enhancement, on both the Stokes and anti-Stokes lines at 1800 $cm^{-1}$, by as much as ~22.8 times and ~3.6 times larger than that provided by a bowtie structure alone. These outstanding results collectively suggest their potential application for new measurement techniques for multiple Raman scattering enhancement and even for broadband Raman enhancement.

## Acknowledgments

Jiao Lin wants to acknowledge Yungui Ma for his helpful discussions. The authors acknowledge the partial support by the National High Technology Research and Development Program (863) of China (No. 2013AA014401), the National Natural Science Foundation of China (nos. 91233208, 61108022, 61271016 and 61178062), and the 111Project. Swedish VR grant (# 621-2011-4620) and AOARD are also acknowledged.

## References

[1] Raman C V 1928 A new radiation *Indian J. Phys.* **2** 387
[2] Nafie L A 2013 Recent advances in linear and nonlinear Raman spectroscopy *J. Raman Spectrosc.* **44** 1629
[3] Kneipp K, Moskovits M and Kneipp H 2006 *Surface-Enhanced Raman Scattering: Physics and Applications* (Berlin: Springer)
[4] Le Ru E and Etchegoin P 2008 *Principles of Surface-Enhanced Raman Spectroscopy and Related Plasmonic Effects* (Amsterdam: Elsevier)
[5] Maier S A 2007 *Plasmonics: Fundamentals and Applications* (Berlin: Springer)
[6] Jeanmaire D L and Van Duyne R P 1977 Surface Raman spectroelectrochemistry: I. Heterocyclic, aromatic, and aliphatic amines adsorbed on the anodized silver electrode *J. Electroanal. Chem. Interfacial Electrochem.* **84** 1
[7] Fleischmann M, Hendra P J and McQuillan A J 1974 Raman spectra of pyridine adsorbed at a silver electrode *Chem. Phys. Lett.* **26** 163
[8] Moskovits M 1985 Surface-enhanced spectroscopy *Rev. Mod. Phys.* **57** 783
[9] Vo-Dinh T 1998 Surface-enhanced Raman spectroscopy using metallic nanostructures1 TrAC *Trends Anal. Chemistry* **17** 557
[10] Fan M, Andrade G F S and Brolo A G 2011 A review on the fabrication of substrates for surface enhanced Raman

spectroscopy and their applications in analytical chemistry *Anal. Chim. Acta* **693** 7
[11] Lin J, Zhang Y, Qian J and He S 2014 A nano-plasmonic chip for simultaneous sensing with dual-resonance surface enhanced Raman scattering and localized surface plasmon resonance *Laser Photon. Rev.* **8** 610
[12] Hatab N A, Hsueh C-H, Gaddis A L, Retterer S T, Li J-H, Eres G, Zhang Z and Gu B 2010 Free-standing optical gold bowtie nanoantenna with variable gap size for enhanced Raman spectroscopy *Nano Lett.* **10** 4952
[13] Roxworthy B J, Ko K D, Kumar A, Fung K H, Chow E K C, Liu G L, Fang N X and Toussaint K C 2012 Application of plasmonic bowtie nanoantenna arrays for optical trapping, stacking and sorting *Nano Lett.* **12** 796
[14] Dodson S, Haggui M, Bachelot R, Plain J, Li S and Xiong Q 2013 Optimizing electromagnetic hotspots in plasmonic bowtie nanoantennae *J. Phys. Chem. Lett.* **4** 496
[15] Schraml K, Spiegl M, Kammerlocher M, Bracher G, Bartl J, Campbell T, Finley J J and Kaniber M 2014 Optical properties and interparticle coupling of plasmonic bowtie nanoantennas on a semiconducting substrate *Phys. Rev.* B **90** 035435
[16] Ikeda K, Takase M, Sawai Y, Nabika H, Murakoshi K and Uosaki K 2007 Hyper-Raman scattering enhanced by anisotropic dimer plasmons on artificial nanostructures *J. Chem. Phys.* **127** 111103
[17] Kelley A M 2010 Hyper-Raman scattering by molecular vibrations *Annu. Rev. Phys. Chem.* **61** 41
[18] Dakin J P, Pratt D J, Bibby G W and Ross J N 1985 Distributed optical fiber Raman temperature sensor using a semiconductor light source and detector *Electron. Lett.* **21** 569
[19] Maher R C, Galloway C M, Le Ru E C, Cohen L F and Etchegoin P G 2008 Vibrational pumping in surface enhanced Raman scattering (SERS) *Chem. Soc. Rev.* **37** 965
[20] Chu Y and Crozier K B 2009 Experimental study of the interaction between localized and propagating surface plasmons *Opt. Lett.* **34** 244
[21] Ghoshal A, Divliansky I and Kik P G 2009 Experimental observation of mode-selective anticrossing in surface-plasmon-coupled metal nanoparticle arrays *Appl. Phys. Lett.* **94** 171108
[22] Ding P, Liang E, Cai G, Hu W, Fan C and Xue Q 2011 Dual-band perfect absorption and field enhancement by interaction between localized and propagating surface plasmons in optical metamaterials *J. Opt.* **13** 075005
[23] Schwind M, Kasemo B and Zorić I 2013 Localized and propagating plasmons in metal films with nanoholes *Nano Lett.* **13** 1743
[24] Lumerical Solutions, Inc. FDTD SOLUTIONS (www.lumerical.com/tcad-products/fdtd/)
[25] Johnson P B and Christy R-W 1972 Optical constants of the noble metals *Phys. Rev.* B **6** 4370
[26] Dos Santos D P, Andrade G F S, Brolo A G and Temperini M L A 2011 Fluctuations of the Stokes and anti-Stokes surface-enhanced resonance Raman scattering intensities in an electrochemical environment *Chem. Commun.* **47** 7158
[27] Dos Santos D P, Temperini M L A and Brolo A G 2012 Mapping the energy distribution of SERRS hot spots from Anti-Stokes to Stokes intensity ratios *J. Am. Chem. Soc.* **134** 13492
[28] Liu Y, Xu S, Li H, Jian X and Xu W 2011 Localized and propagating surface plasmon co-enhanced Raman spectroscopy based on evanescent field excitation *Chem. Commun.* **47** 3784
[29] Prodan E, Radloff C, Halas N J and Nordlander P 2003 A Hybridization model for the plasmon response of complex nanostructures *Science* **302** 419
[30] Ahmed A and Gordon R 2011 Directivity enhanced Raman spectroscopy using nanoantennas *Nano Lett.* **11** 1800
[31] Wang D, Zhu W, Chu Y and Crozier K B 2012 High directivity optical antenna substrates for surface enhanced Raman scattering *Adv. Mater.* **24** 4376